IET Generation, Transmission & Distribution

Research Article

IET Journals
The Institution of Engineering and Technology

Controlling the thermal environment of underground cable lines using the pavement surface radiation properties

ISSN 1751-8687
Received on 23rd August 2017
Revised 2nd March 2018
Accepted on 29th March 2018
E-First on 3rd May 2018
doi: 10.1049/iet-gtd.2017.1298
www.ietdl.org

Dardan Klimenta[1] ✉, Bojan Perović[1], Jelena Klimenta[2], Milena Jevtić[3], Miloš Milovanović[1], Ivan Krstić[1]

[1]*Faculty of Technical Sciences, University of Priština in Kosovska Mitrovica, Kneza Miloša St. 7, RS-38220 Kosovska Mitrovica, Serbia*
[2]*Independent Consultant in the Field of Urban and Spatial Planning, Bul. Dr Zorana Đinđića St. 125, RS-18108 Niš, Serbia*
[3]*Technical Faculty in Bor, University of Belgrade, Vojske Jugoslavije St. 12, RS-19210 Bor, Serbia*
✉ *E-mail: dardan.klimenta@pr.ac.rs*

Abstract: The main purpose of this study is to show how the emissivity and absorptivity of a pavement surface above underground cables affect their ampacity. The use of cool pavements whose surfaces absorb less heat from the Sun than they emit to the ambient is considered as a novel method to control the thermal environment of underground cables. The method predicts that the trench along the entire length of a 110 kV cable line is completely filled with quartz sand and paved with a cool pavement. Quartz sand would provide good conduction of heat from the cables to the earth and pavement surfaces, while a paved surface of the trench would establish approximately unchangeable convection and radiation boundary conditions along the entire cable line route. It is assumed that the three-phase system is balanced and that the boundary conditions along the earth and pavement surfaces are the most unfavourable. The novel method is based on the results of experimental research, generalised and verified numerically using the finite-element method in COMSOL. Finally, it is established that the ampacity of the 110 kV cable line can be increased up to 26.7%.

1 Introduction

The ampacities of underground cable lines in distribution networks are very sensitive to changes in the surrounding thermal environments. The soil parameters affecting the cable ampacity are thermal conductivity, thermal diffusivity and soil temperature. It is possible to control these parameters using special cable beddings and systems for forced cooling or irrigation of cable beddings. So, there is a possibility to change the thermal conductivity and diffusivity of soils using special cable beddings, the soil temperature using systems for forced cooling, and all the three parameters using systems for irrigation.

The existing literature in English currently does not identify pavement surfaces as means to control the thermal properties of the environment around the underground power cables. The effect of the paved surface of the earth on the ampacity of an underground cable line usually comes down to the natural convection boundary condition [1] or to a combination of the natural convection and radiation boundary conditions by accounting for the influence of solar heating [2]. However, there is a possibility to change temperatures of cables, bedding and surrounding soil by the radiation properties of pavement surface.

For standard ways of laying cables, directly in the soil or in the dimensionally optimised cable bedding, conduction of heat between the cables and the paved surface of the earth is not the best possible one. The best possible transfer of heat between the cables and the air contacting the pavement would be ensured by filling the cable trench completely with bedding containing a high amount of quartz or with pure quartz sand. In this case, it is recommended to optimise only the width of the cable bedding (or the width of the trench) and consider the paved surface of the earth as a mean to control the thermal environment of cables. In practice, soils under pavements are usually almost completely dried-out so that the changes in boundary conditions along the earth surface and solar radiation can only affect the soil temperature. The thermal conductivity and diffusivity of soils are inconsiderably affected by these changes.

This paper is based on the experimental results obtained using an apparatus consisted of a round tubular heater inside a copper pipe acting as (on an approximate scale) a single AXLJ $1\times 1000/190$ mm^2 110 kV cable, a thermally insulated container, a temperature regulation system, river sand acting as the cable bedding, concrete blocks acting as the pavement, a data acquisition system and two multi-meters. The experiments were performed in a laboratory. This means that the effect of the Sun was excluded. However, the thermal effect of the laboratory interior on the surface of the concrete blocks in the experimental apparatus is equivalent to the thermal effect of outdoor solar radiation, because of which it was not necessary to carry out outdoor experiments. Also, the effect of the Sun is subsequently added through a numerical simulation of the problem with the single 110 kV cable and experimentally determined boundary conditions. In addition, the results are generalised to the case of an underground 110 kV cable line. It is assumed that 110 kV cables will be installed in trefoil formation where the axial spacing between the individual cables equals one cable diameter, i.e. in accordance with the relevant standards. Moreover, it is assumed that the soil temperature at a reference distance is 20°C [3].

The effect of the pavement surface radiation properties on the distribution 110 kV cable line is then analysed. This paper also describes the conditions under which a pavement surface may be used as a mean to control the thermal environment around the cables, as well as their ampacity. Furthermore, there was no optimisation of the cable bedding size, but it is assumed that the width of the soil zone intended for laying cables equals 1.2 m. According to the DIN VDE standards, the AXLJ $1\times 1000/190$ mm^2 110 kV cables considered herein correspond to the NA2XS(FL)2Y type.

2 Experimental apparatus and procedure

2.1 Apparatus and materials

Photographs of the experimental apparatus are shown in Fig. 1. The photographs illustrate the following experimental cases: (a) without the soil environment, (b) pavement made of concrete blocks covered by some river sand acting as dust, (c) concrete pavement coated with acrylic white paint and (d) concrete pavement coated with acrylic black paint. The absorptivity α and emissivity ε of concrete surface and acrylic paints, together with

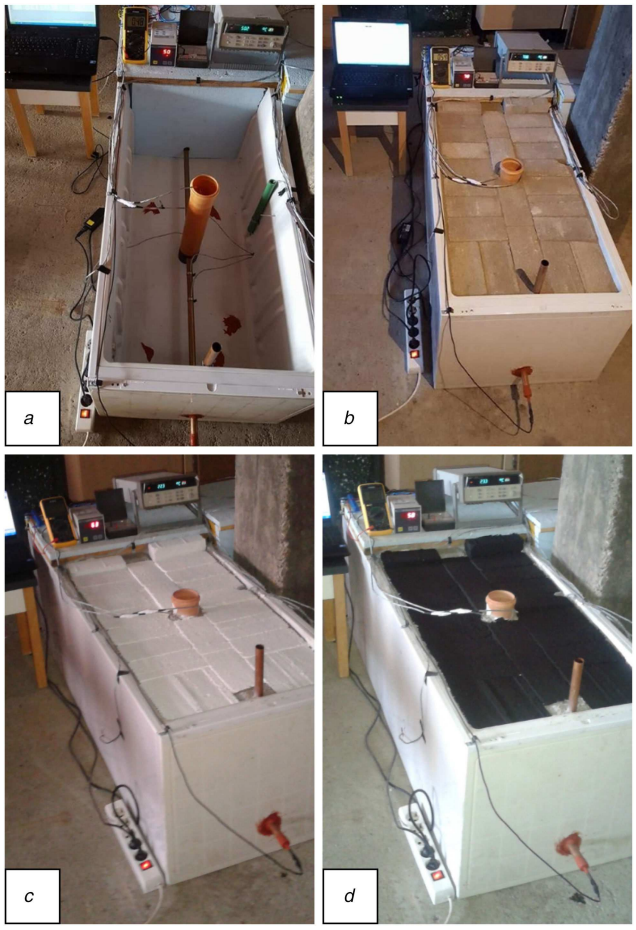

Fig. 1 *Photographs of the experimental apparatus*
(a) Without the soil environment, ***(b)*** With a grey and dusty pavement surface, ***(c)*** With a white pavement surface, ***(d)*** With a black pavement surface

the radiation properties of some other materials and paints (which can also be used for controlling the thermal environment of underground cables), are listed in Table 1.

The purpose of this apparatus is to simulate the effects of the pavement surface emissivity and absorptivity on the thermal environment of underground power cables under known ambient conditions in a laboratory, where the effect of the inner walls of that laboratory was equivalent to the effect of outdoor solar radiation. This will be explained further in Section 4. Fig. 2 illustrates the schematic diagram of the experimental apparatus.

The apparatus was composed of a container made from a used refrigerator, whose walls consisted of 2-mm-thick polystyrene inside, 1-mm-thick low-carbon steel on the outside, with 47- or 57-mm-thick polyurethane foam between as a thermal insulation (Fig. 1). One side of the container was constructed of 50-mm-thick polyurethane foam slab sandwiched between two 30-mm-thick slabs of styrodur. The container had a height of 0.5 m, a width of 0.6 m and a length of 1.17 m. It was filled with river sand up to 0.075 m below the top edges of the container. River sand reproduces, on an approximate scale, the cable bedding, while inner surfaces of the container represent the bedding edges. For all the outer surfaces of the container (four lateral and one bottom), it was found that the heat transfer coefficient amounts ∼3 W m^{-2} K^{-1}. Table 2 presents thermal conductivities k of materials used for experiments and for later simulations.

The actual AXLJ $1 \times 1000/190\ mm^2$ 110 kV cable was modelled by an uninsulated copper pipe of a smaller outer diameter, which was also equipped with an overflow pipe. A round tubular heater having a total nominal power of 800 W and a length of 1.3 m was mounted in the centre of the copper pipe. The heater was connected to the low-voltage power supply network by means of a microprocessor-based temperature regulator (NIGOS 1011P) and an auxiliary relay (SCHRACK multimode relay MT 326230), as shown in Fig. 2. The space between the heater and the inner surface of the copper pipe was filled with mineral motor oil.

In these experiments, the J-type thermocouples were installed on the copper pipe in four different locations (P1 in the air, and P2–P4 in the sand), including the inner lateral surface of the container (P5), the lower surface of the pavement (P6), the upper surface of the pavement (P7), and the air surrounding the apparatus (P8). The thermocouple P1 was directly connected to the measuring input of temperature regulator. The temperatures measured by the thermocouples P2–P8 were collected through a data acquisition system (Agilent 34970A) that was connected to a laptop to collect the data. Temperatures of the outer lateral surfaces of the container were measured by an infrared thermometer with an accuracy of ±2.0°C below and above 100°C. There was also one Pt100 temperature sensor to monitor the internal temperature in the module of the data acquisition system, which is used as a reference/cold junction temperature.

2.2 Procedure

The heater was operated with 220 V, 3.31 A and 50 Hz. During the runs with the empty container, the FLIR i3 thermal imaging camera was used for inspection of the heater and for selection of the positions for the thermocouples P1–P4 on the copper pipe. This is due to the fact that a round tubular heater uses a single or several strands of wire to transfer heat to arc areas of its round tube, which provides no-uniform heating throughout the surface of the tube. Some thermal images confirming this fact are shown in Fig. 3. Based on this inspection, the selection of the positions P1–P4 was made as shown in Fig. 2. The temperatures of the copper pipe at points P2–P4 were controlled by adjusting the temperature at point P1 with an error <1°C for environmental temperatures between 0 and 50°C. Temperature of the outer surface of the copper pipe part enclosed by the vertical plastic pipe was fixed at 61, 66 and 71°C (a specified control temperature).

When the container was empty, the points at which the temperatures were lower than the corresponding adjusted value were selected for the thermocouples P2–P4. Then, after the addition of sand, the temperatures at points P2–P4 were increased by a few degrees Celsius adjusting the thermal environment as closely as possible in accordance with the temperature at point P1. This is expected because the convection and radiation on the outer surface of the copper pipe were replaced by conduction alone. Along with application for the controlling, the thermocouple P1 was also used for measurement of the corresponding temperature. The temperature of the air surrounding the apparatus was adjusted at 23°C with an accuracy of ±1.5°C.

In order to study the steady-state temperature distribution for different pavement surfaces and known laboratory conditions, temperatures at 8 h from the start of each experiment were noted. One test ended once a period of 8 h has elapsed. The actual effect of the Sun is subsequently defined and added through numerical simulations of the problem with experimentally determined boundary conditions.

3 Case studies

3.1 Governing equation

In this paper, the authors consider two cases of steady-state thermal analysis, using the indoor/laboratory ambient conditions and the most unfavourable outdoor ambient conditions. The steady-state thermal finite-element method (FEM) models and associated analysis are based on the following partial differential equation [4, 5]:

$$\frac{\partial}{\partial x}\left(k\frac{\partial T}{\partial x}\right)+\frac{\partial}{\partial y}\left(k\frac{\partial T}{\partial y}\right)+Q_v=0 \tag{1}$$

where k is the thermal conductivity in $W\cdot K^{-1}\cdot m^{-1}$, T is the temperature in K, x, y are Cartesian spatial coordinates in m, and Q_v is the volume power of heat sources in $W\cdot m^{-3}$. Although (1) is

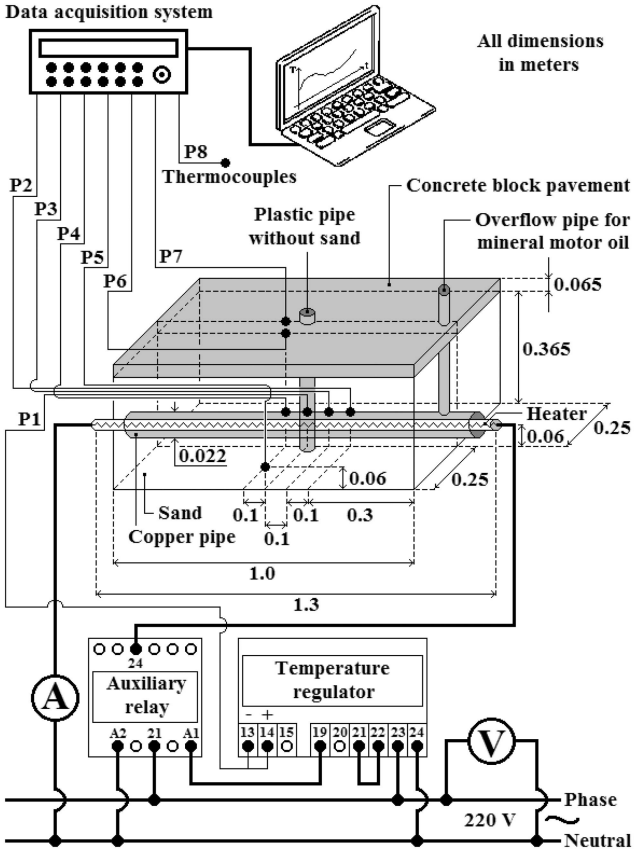

Fig. 2 *Schematic diagram of the experimental apparatus*

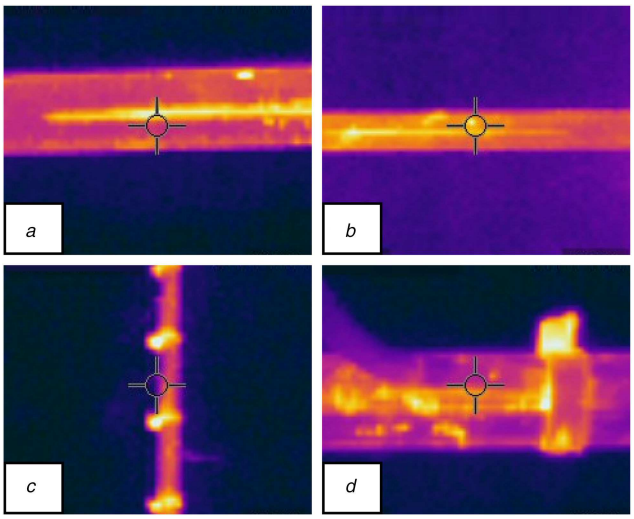

Fig. 3 *Some thermal images of the experimental apparatus without the soil environment*

(a), ***(b)*** Before installation of the thermocouples P1–P4, ***(c)***, ***(d)*** After installation of the thermocouples P1–P4

written as a linear equation, thermal FEM simulations will be non-linear due to the radiation boundary condition.

3.2 Computational domains

Computational domains which will be used for confirmation of the initial assumption that the thermal environment of underground cables can be controlled by the paved surface of the earth are given in Figs. 4 and 5.

The computational domain corresponding to the experimental apparatus considered herein is shown in Fig. 4. Fig. 5*a* shows that the computational domain for the case when the cables are laid in the bedding of a standard size, while Fig. 5*b* shows the computational domain for the case when the cable trench is

Table 1 Radiation properties of pavement surfaces and paints

Material or paint	α, —	ε, —
concrete block	0.56–0.69	0.94
acrylic white paint	0.26	0.9
acrylic black paint	0.97	0.91
magnesium oxide white paint	0.09	0.9
magnesium oxide aluminium oxide paint	0.09	0.92
brick, light	0.25–0.36	0.85–0.95
limestone, light	0.33	0.9–0.93
marble, white	0.44	0.9–0.93
limestone, dark	0.53	0.9–0.93
clay tiles, red or brown	0.60–0.69	0.85–0.95
asphalt	0.87	0.93

Table 2 Thermal conductivity of some materials

No.	Material	k W·K^{-1}·m^{-1}
1.	Polystyrene	0.13
2.	low-carbon steel	43
3.	polyurethane foam	0.025
4.	styrodur	0.033
5.	river sand, with particles smaller than 3 mm, 1365 kg m^{-3}	0.4
6.	asphalt, 2300 kg m^{-3}	1.2
7.	brick, light, solid, 2600 kg m^{-3}	1
8.	limestone, light, 2180 kg m^{-3}	1.5
9.	concrete block, 2000 kg m^{-3}	1.3
10.	cable bedding	1
11.	native soil	0.4
12.	aluminium	239
13.	copper	385
14.	PE, HDPE and XLPE	0.286

HDPE, high-density polyethylene.

completely filled with the bedding. Compared with the computational domain in Fig. 4, the dimensions of the domains shown in Fig. 5 are large and selected in accordance with the rule saying that external boundaries of a computational domain should be positioned in places where the constant temperature and homogenous boundary conditions are satisfied simultaneously [6].

For the purposes of simulations using the COMSOL Multiphysics software, the AXLJ 1 × 1000/190 mm^2 110 kV cables are modelled by an equivalent construction composed of the aluminium conductor, cross-linked polyethylene (XLPE) insulation, copper screen and outer polyethylene (PE) sheath with outer diameters d_1, d_5, d_8 and d_9, respectively. According to [6], the equivalent construction is created in the following manner: (i) the semi-conducting screens and swelling tapes under the metal screen are added to the block representing the XLPE insulation and (ii) the swelling tapes over the metal screen and water-sealing aluminium layer are modelled by an equivalent metal screen with thermal properties of copper. The outer diameters d_1–d_9 of all nine construction elements of this cable are given in Fig. 6.

FEM simulations of temperature field distributions over the domain shown in Fig. 4 are conducted for pavement made of concrete blocks covered by some river sand acting as dust, concrete pavement coated with acrylic white paint and concrete pavement coated with acrylic black paint. Simulations over the domains shown in Fig. 5 are conducted for the following five pavements: asphalt coated with magnesium oxide white paint, light bricks, light limestone, concrete blocks and uncoated asphalt. The pavement materials are selected so that their solar absorptivities and emissivities are assumed to be equal to the lower bounds of the corresponding ranges of possible values from Table 1. It is also

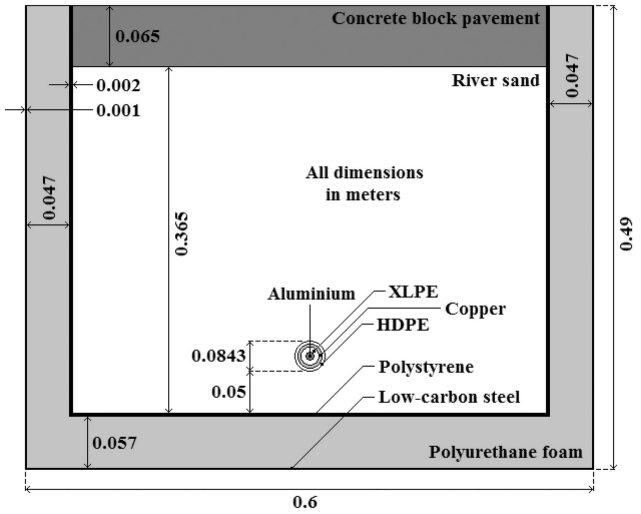

Fig. 4 *Computational domain corresponding to the experimental apparatus*

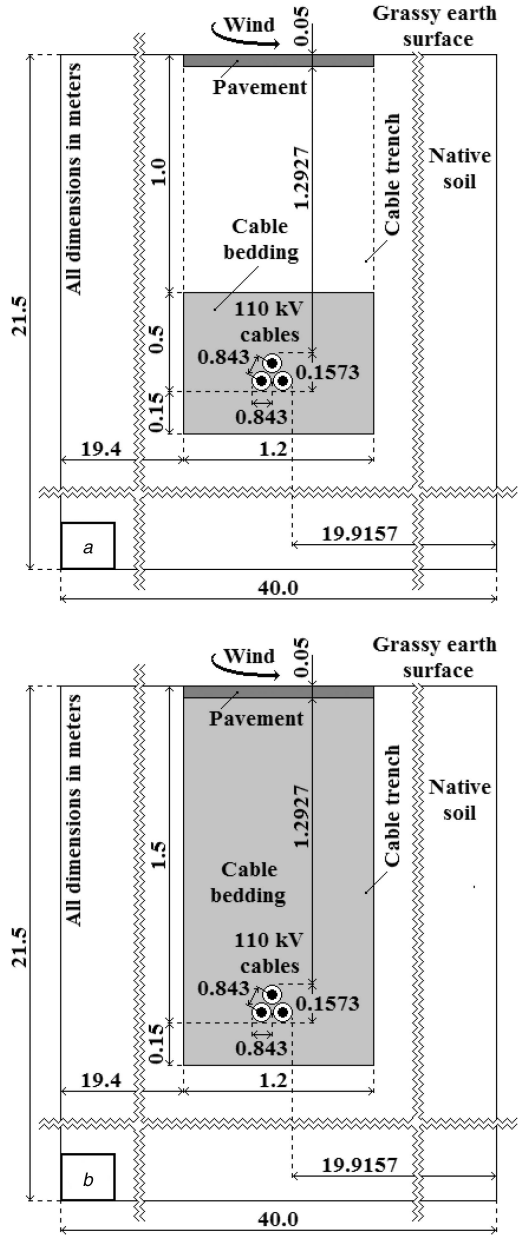

Fig. 5 *Computational domains for the cases of cable bedding sizes* ***(a)*** 1.2 m × 0.65 m, ***(b)*** 1.2 m × 1.6 m

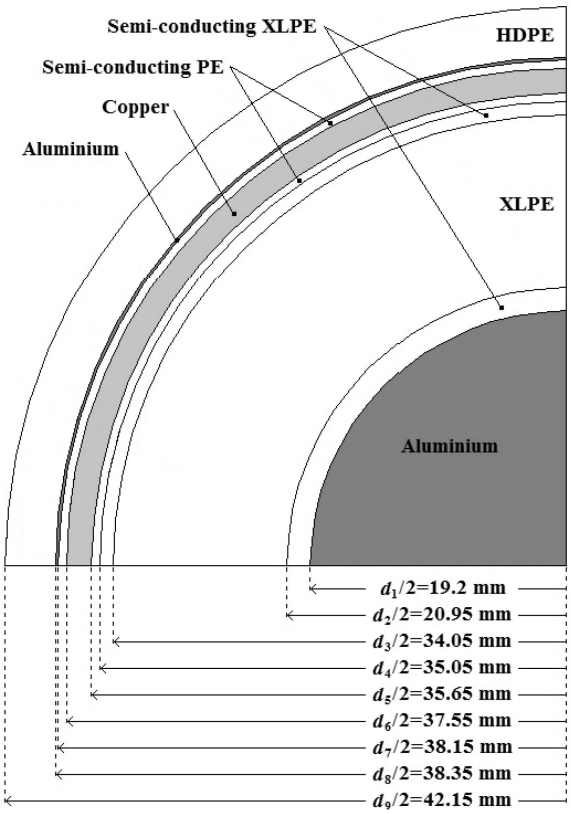

Fig. 6 *Dimensions of the construction elements of the AXLJ 1 × 1000/190 mm² 110 kV cable*

assumed that the pavement thickness equals 0.05 m for each of the five materials and that there are grassy areas on the both sides of the pavement.

3.3 Material properties and heat sources

The thermal conductivities k of all the materials and the electrical conductivity of aluminium ρ_e are necessary for the steady-state thermal FEM analysis. All the necessary material properties required by this analysis are constant and selected so that the obtained results are optimistic from the engineering point of view. Hence, the values of the thermal and electrical properties which correspond, respectively, to the associated dried-out states (of the native soil and the cable bedding) and the continuously permissible temperature T_{cp} are taken into consideration. Continuously permissible temperature of the considered XLPE cables is $T_{cp} = 90°C$. The values for k are taken from related literature and represented in Table 2.

The volume power of heat sources located in the conductor Q_v with a diameter of $d_1 = 38.4 \times 10^{-3}$ m and with a geometric cross-section area of $S_c' = 1158.117 \times 10^{-6}\,\text{m}^2$ is

$$Q_v = \frac{R_{ac}(T_{cp})}{S_c'} \cdot I^2 \tag{2}$$

where $R_{ac}(T_{cp}) = 4.091094 \times 10^{-5}\,\Omega\,\text{m}^{-1}$ is the ac resistance per unit length of the conductor at temperature T_{cp}, and I is the load current in A. The a.c. resistance of the 110 kV cables is calculated taking into account the skin and proximity effects [6].

Volume powers of heat sources located in the cable insulations are equal to zero due to the fact that, in accordance with the IEC 60287 standard, the associated dielectric losses are negligible for 110 kV cables. According to [6, 7], the dielectric losses per unit length in each phase are equal to $0.362647\,\text{W}\cdot\text{m}^{-1}$. The influence of these losses is added to the losses in conductors of the cables. Volume powers of heat sources located in the metal screens of the

110 kV cables are also equal to zero because of the cross-bonding of metal screens [6].

3.4 Boundary conditions

It is common to determine the cable ampacity I_{cp} for the most unfavourable ambient conditions such as (i) temperature of the air contacting the earth surface $T_a = 40°C$; (ii) wind velocity, i.e. velocity of the air near the earth surface of $v_a = 0.22\ m \cdot s^{-1}$; (iii) solar irradiance incident on the earth surface $Q_{S,s} = 1000\ W\ m^{-2}$; and (iv) thermal conductivities of the cable bedding and native soil whose values correspond to their dried-out states, i.e. 1 and 0.4 W $K^{-1}\ m^{-1}$, respectively. Thus, the 110 kV cables will be analysed under the experimentally determined boundary conditions and under the most unfavourable ones.

A homogenous boundary condition is used to model boundaries surrounding the left-hand, right-hand and bottom sides of the computational domains in Fig. 5 (with regard to the earth surface), where a constant temperature boundary condition also needs to be satisfied simultaneously [6]. When taking into account the homogenous boundary condition, the value of the heat flux per unit area amounts zero [6].

In all three case-studies under consideration, the heat transfer along the earth and pavement surfaces is represented by a combination of the following boundary conditions:

- The constant heat flux boundary condition [8]:

$$k \cdot \frac{\partial T}{\partial n} = -\alpha \cdot Q_{S,s} \tag{3}$$

- The convection boundary condition [8]:

$$k \cdot \frac{\partial T}{\partial n} = h \cdot (T - T_a) \tag{4}$$

- The radiation boundary condition: (i) the radiation emitted by the earth surface is less than the radiation emitted by a black body at the same temperature T, and is expressed as [9]

$$k \cdot \frac{\partial T}{\partial n} = \varepsilon \cdot \sigma_{SB} \cdot T^4; \tag{5}$$

(ii) When the pavement surface of the experimental apparatus at a temperature T is completely enclosed by a much larger surface of the laboratory at temperature T_a separated by the air that does not intervene with radiation, the net radiation heat flux between these two surfaces is given as [8, 9]

$$k \cdot \frac{\partial T}{\partial n} = \varepsilon \cdot \sigma_{SB} \cdot (T^4 - T_a^4); \tag{6}$$

where $\alpha = 0.6$ and $\varepsilon = 0.94$ for a dry grassy surface [10–12], $h = 12.654\ W\ K^{-1} \cdot m^{-2}$ for a dry grassy surface when $v_a = 0.22\ m\ s^{-1}$ [12, 13], $h = 8\ W\ K^{-1}\ m^{-2}$ for a pavement surface when $v_a = 0.22\ m\ s^{-1}$ [6, 12] and $\sigma_{SB} = 5.67 \times 10^{-8}\ W\ m^{-2}\ K^{-4}$ is the Stefan–Boltzmann constant. The coefficient h, which appears in (4), takes into account heat transfer due to convection between the earth surface and the ambient air. The other values for the coefficients α and ε are given in Table 1.

It is assumed in this paper that the convection coefficient for a grassy surface has a greater value than the one for a pavement surface. This is caused by some loss of heat due to evaporation of water from the grassy surfaces, which does not exist along the pavement surfaces [12, 14]. Therefore, the effect of evaporation on the heat transfer due to convection between the earth surface and the ambient air is introduced by the corresponding coefficient, whose value is calculated using the empirical correlations from [13] and adjusted in accordance with the experimental results reported in [12].

4 Results and discussion

4.1 Experimental results

The temperatures at points P1–P8 and the average temperature of the outer lateral surface of the container obtained for the four cases (a–d) illustrated by Fig. 1 are listed in Table 3. Table 3 also contains the specified control temperature and the average temperature of the outer surface of the copper pipe (obtained by averaging the measured values at points P2, P3 and P3).

4.2 Validation of the method

The results obtained by simulating the temperature field distribution over the two-dimensional domain in Fig. 4 are reported in Table 4. This table outlines the main results obtained for the actual indoor/laboratory conditions. The temperature differences between the simulation results from Table 4 and corresponding experimental values from Table 3 are listed in Table 5. For the domain shown in Fig. 4, a sequence of simulations is performed with grey, white and black pavement surfaces. The appearance order of the colours in Tables 4 and 5 follows the sequence of experiments (as in Fig. 1). The surface radiation properties and thermal conductivities appearing in this FEM model are given in Tables 1 and 2, respectively.

When the simulation results from Table 4 are compared with the corresponding experimental data in Table 3, the following observations can be made: (i) For each temperature of the cable conductor, under known indoor/laboratory conditions, approximately the same load current is obtained regardless of the colour of the pavement surface. (ii) The calculated temperature of the outer surface of the 110 kV cable $T_{c,os}$ is lower by 0.2–1.1°C than the corresponding average temperature of the outer surface of the copper pipe. (iii) The difference between the calculated temperature of the lower surface of the pavement and its corresponding measured value at point P6 ranges from +0.84 to +4.25°C. (iv) The difference between the calculated temperature of the upper surface of the pavement and its corresponding measured value at point P7 ranges from −0.13 to +2.9°C. The first observation is based on approximately equal values for the emissivity of the three colours, while the remaining three observations indicate a satisfactory level of accuracy on account of the created model.

The thermal effect of the laboratory interior on the surface of the pavement in the experimental apparatus is equivalent to the thermal effect of outdoor solar radiation. For the grey, white or black surface the product $\alpha \cdot Q_{S,s}$ equals 409.98, 392.52 or 396.89 W m^{-2}, respectively. This means that the results from Table 4 would also be obtained in the case that the experimental apparatus was located outdoors and that the solar irradiance $Q_{S,s}$ corresponding to the previously given products $\alpha \cdot Q_{S,s}$ was incident on the pavement surface. If $Q_{S,s}$ was 0 W m^{-2}, a significantly larger load current would correspond to each particular case from Table 4. In the cases of grey, white and black surfaces when $Q_{S,s} = 0\ W\ m^{-2}$, the following values of load currents would be, respectively, obtained: 1020.31, 1014.61 and 1016 A – for $T_{c,os} = 60°C$; 1063.31, 1057.84 and 1059.18 A – for $T_{c,os} = 65°C$; and 1104.64, 1099.31 and 1100.66 A – for $T_{c,os} = 70°C$. Accordingly, the variation of the load current follows the change in the emissivity. In particular, with the exclusion of solar radiation, the load currents can be increased up to 25%. Thus, it appears that this would be the most adequate manner to quantify the effect of the pavement surface absorptivity (i.e. solar radiation) on the load current (i.e. ampacity).

How the solar absorptivity of the pavement surfaces affects the conductor temperature and load current of the 110 kV cable can best be illustrated by concrete examples of the temperature field distribution over the computational domain in Fig. 4. Accordingly, Figs. 7*a* and *b* show the temperature field distribution over this computational domain for the grey pavement surface excluding and including the effect of the Sun, respectively. The two cases presented in Fig. 7 are selected so that the volume power of heat sources (located in the conductor) Q_v corresponds to the outer surface temperature of the cable $T_{c,os} = 70°C$. Also, the temperature

Table 3 Experimental results

Point or outer surface	Specified control temperature					
	61°C	66°C	71°C	61°C	66°C	71°C
	Measured temperature, °C					
		Case (a)			Case (b)	
P1	60.0	65.0	70.0	60.0	65.0	70.0
P2	55.7	59.5	63.9	58.5	62.9	67.7
P3	57.6	61.6	65.9	60.0	64.4	69.4
P4	59.5	64.6	68.6	63.4	68.4	73.9
copper pipe[a]	57.6	61.9	66.1	60.6	65.2	70.3
P5	24.4	23.7	24.3	29.8	31.4	33.0
container[a]	23.5	23.1	23.0	22.4	22.6	22.4
P6	—	—	—	24.2	24.8	24.6
P7	—	—	—	23.5	23.8	23.6
P8	23.1	22.7	22.7	21.6	21.8	21.5
		Case (c)			Case (d)	
P1	60.0	65.0	70.0	60.0	65.0	70.0
P2	58.9	63.5	68.1	58.9	63.4	68.0
P3	60.3	65.1	69.9	60.2	64.9	69.7
P4	64.0	69.2	74.6	63.8	69.0	74.4
copper pipe[a]	61.1	65.9	70.9	61.0	65.8	70.7
P5	32.2	32.3	33.6	32.6	33.3	34.3
container[a]	23.9	24.6	24.3	24.2	24.4	24.2
P6	24.9	26.9	26.9	26.8	27.3	27.1
P7	23.5	26.2	25.9	25.9	26.3	25.9
P8	23.0	24.2	23.2	22.8	23.8	22.7

[a]Average values.

Table 4 Simulation results obtained for the actual indoor/laboratory conditions, i.e. for $T_a = 23°C$, $v_a = 0\ m \cdot s^{-1}$, $h = 7.382\ W\ m^{-2}\ K^{-1}$ and $Q_{S,s} = 0\ W\ m^{-2}$

Pavement surface		Temperature, °C				Q_v, W·m^{-3}	I, A
		Cable conductor	$T_{c,os}$, °C	Pavement			
Colour	ε, —			Lower surface	Upper surface		
grey	0.94	71.31	60.00	27.61	25.76	23,555	816.58
white	0.90	71.30	60.00	27.65	25.81	23,535	816.23
black	0.91	71.30	60.00	27.64	25.79	23,540	816.32
grey	0.94	77.83	65.00	28.23	26.13	26,735	869.95
white	0.90	77.82	65.00	28.28	26.18	26,715	869.63
black	0.91	77.82	65.00	28.26	26.17	26,720	869.71
grey	0.94	84.35	70.00	28.85	26.50	29,915	920.24
white	0.90	84.33	70.00	28.90	26.56	29,890	919.86
black	0.91	84.34	70.00	28.89	26.54	29,895	919.93

Table 5 Temperature differences between the simulated and experimental values calculated for the actual indoor/laboratory conditions, i.e. for $T_a = 23°C$, $v_a = 0\ m \cdot s^{-1}$, $h = 7.382\ W \cdot m^{-2} \cdot K^{-1}$ and $Q_{S,s} = 0\ W \cdot m^{-2}$

Pavement surface		Temperature difference, °C		
		Cable outer surface	Pavement	
Colour	ε, —		Lower surface	Upper surface
grey	0.94	−0.6	+3.41	+2.26
white	0.90	−1.1	+2.75	+2.31
black	0.91	−1.0	+0.84	−0.11
grey	0.94	−0.2	+3.43	+2.33
white	0.90	−0.9	+1.38	−0.02
black	0.91	−0.8	+0.96	−0.13
grey	0.94	−0.3	+4.25	+2.90
white	0.90	−0.9	+2.00	+0.66
black	0.91	−0.7	+1.79	+0.64

field distribution obtained for the actual indoor conditions is the same as for the equivalent outdoor conditions, i.e. for $T_a = 23°C$, $v_a = 0\ m\ s^{-1}$, $h = 7.382\ W\ m^{-2}\ K^{-1}$, $\alpha = 0.56$, $Q_{S,s} = 732.11\ W\ m^{-2}$, $\varepsilon = 0.94$ and $Q_v = 29{,}915\ W\ m^{-3}$. In addition, it can be noticed that the increase of the solar irradiance from 732.11 to 1000 W m^{-2} leads to a reduction in the load current from 920.24 to 848.62 A.

4.3 Generalisation of the method

In order to generalise the previous results, the two large-size FEM models with 110 kV cables were created and represented geometrically in Fig. 5. The temperature field distributions over these computational domains are also calculated. For each of these two domains, a sequence of simulations is performed with the following five materials: asphalt coated with magnesium oxide white paint, light bricks, light limestone, concrete blocks and uncoated asphalt. The surface radiation properties and thermal conductivities of these materials are listed in Tables 1 and 2, respectively.

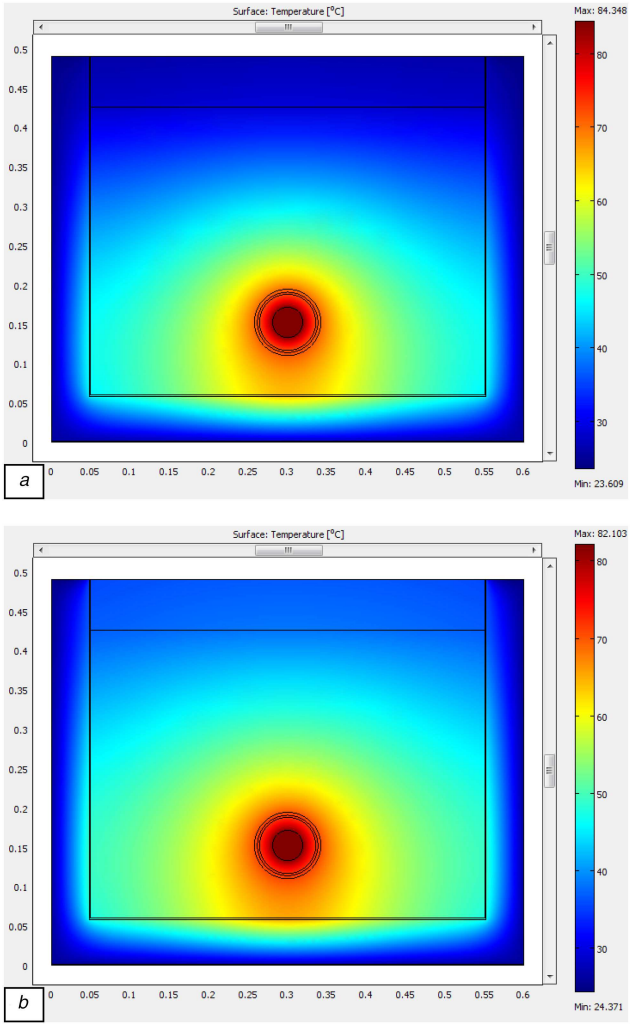

Fig. 7 *Temperature field distributions over the computational domain shown in Fig. 4*

(a) Actual indoor conditions, i.e. for $T_a = 23°C$, $v_a = 0\ m\ s^{-1}$, $h = 7.382\ W\ m^{-2}\ K^{-1}$, $Q_{S,s} = 0\ W\ m^{-2}$, $\varepsilon = 0.94$ and $Q_V = 29{,}915\ W\ m^{-3}$, ***(b)*** Outdoor conditions similar to the actual ones in the laboratory, i.e. for $T_a = 23°C$, $v_a = 0\ m\ s^{-1}$, $h = 7.382\ W\ m^{-2}\ K^{-1}$, $Q_{S,s} = 1000\ W\ m^{-2}$, $\alpha/\varepsilon = 0.596$ and $Q_V = 25{,}440\ W\ m^{-3}$, where all dimensions are in meters

For the two large-size domains, values for Q_V and I_{cp} are selected in such a way so that they correspond to asphalt surface radiation properties from Table 1, thermal conductivity of the asphalt $k = 1.2\ W\ K^{-1}\cdot m^{-1}$ and continuously permissible temperature of the cables $T_{cp} = 90°C$, as follows: $Q_V = 10{,}250\ W\ m^{-3}$ and $I_{cp} = 538.665\ A$ – for the domain in Fig. 5*a*, and $Q_V = 11{,}260\ W\ m^{-3}$ and $I_{cp} = 564.58\ A$ – for the domain in Fig. 5*b*. The remaining input parameters are constant and specified in the preceding sections.

The next aim is to demonstrate how the radiation properties of the pavement surface affect the temperatures of the pavement, bedding and cables' conductors for the cases when the cable trench is partly (the bedding is of a standard size) and completely filled with the bedding material. The temperatures of the pavement, bedding and conductors which are obtained by simulations of the temperature field distribution over the domains in Figs. 5*a* and *b* are listed in Tables 6 and 7, respectively.

Based on the results presented in Tables 6 and 7, it can be seen that the temperatures of the pavement, bedding and cables' conductors decrease with decreasing the ratio of absorptivity to emissivity α/ε for the pavement surface. The same applies to both the large-size domains considered herein. Hence, it is possible to increase the cable ampacity by selecting a material or paint with a lower value of the ratio α/ε. The effect of the ratio α/ε on the cable ampacity will be quantified and presented later in this section.

Table 6 Effect of pavement surface radiation properties on temperatures of pavement, bedding and conductors for the computational domain in Fig. 5*a*

Pavement material	Surface radiation property α/ε, —	Temperatures for $Q_V = 10{,}250\ W\cdot m^{-3}$, i.e. $I_{cp} = 538.665\ A$		
		Pavement surface, °C	Bedding close to cables, °C	Cables' conductors, °C
asphalt + paint	0.100	12.01	70.32	75.68
brick, light	0.294	25.48	74.04	79.45
limestone, light	0.367	29.60	75.12	80.47
concrete block	0.596	43.83	79.09	84.45
asphalt	0.935	63.78	84.63	90.00

Table 7 Effect of pavement surface radiation properties on temperatures of pavement, bedding and conductors for the computational domain in Fig. 5*b*

Pavement material	Surface radiation property α/ε, —	Temperatures for $Q_V = 11{,}260\ W\cdot m^{-3}$, i.e. $I_{cp} = 564.58\ A$		
		Pavement surface, °C	Bedding close to cables, °C	Cables' conductors, °C
asphalt + paint	0.100	13.35	61.57	67.44
brick, light	0.294	26.44	67.52	73.39
limestone, light	0.367	30.43	69.06	74.93
concrete block	0.596	44.29	75.33	81.22
asphalt	0.935	63.80	84.10	90.00

In addition, it is clear from Tables 6 and 7 that the temperatures of the pavement, bedding and cables' conductors would be decreased significantly by the cable bedding made according to Fig. 5*b*. The effect of cable bedding dimensions can also be illustrated using the sizes of the dried and dried-out zones enclosed by the isotherms of 50, 60 and 70°C. According to [3, 6, 15, 16], the temperature of 50°C is singled out as a temperature above which a balance between the dried-out and wet zones shall certainly be established, regardless of the type of bedding/soil. The temperature of 60°C is taken into consideration as a critical temperature for the drying-out process that was commonly used by IEC, CIGRE and IEEE [16]. Moreover, it is assumed that the isotherm of 70°C encloses an extremely dried-out zone.

Therefore, it is interesting to compare the results obtained for the domains in Figs. 5*a* and *b* and for the case when the trench is paved with a cheap and easily available material such as light brick. The isotherms of 50, 60 and 70°C which are obtained by simulation of the steady-state temperature field distribution over the domain in Fig. 5*a* are presented in Fig. 8*a*. Fig. 8*b* shows these isotherms generated within the domain in Fig. 5*b*.

Based on the sizes of the dried, dried-out and extremely dried-out zones shown in Figs. 8*a* and *b*, it is evident that the temperature effect of the cable bedding is higher when it has a smaller size. According to Tables 6 and 7, the effect of the bedding on the cables' conductors, expressed in the form of a temperature difference, amounts to 8.24°C – for the asphalt coated with magnesium oxide white paint, 6.06°C – for the light bricks, 5.54°C – for the light limestone and 3.23°C – for the concrete blocks. This also agrees with the conclusion which is drawn from the results shown in Figs. 8*a* and *b*. For this comparison, it is also important to point out the fact that an extremely dried-out zone does not exist in the result shown in Fig. 8*b*. Namely, according to Fig. 8*b*, the

isotherm of 70°C is divided into three parts (three mutually separated circles) which go through the XLPE insulations of the 110 kV cables (enclosing their conductors).

For the purposes of determining the ampacity of the 110 kV cable line I_{cp}, a sequence of simulations over each of the two computational domains (in Fig. 5) is performed with the radiation and thermal properties (α, ε and k) of the previously selected pavement materials (Tables 6 and 7). The values for Q_v are gradually increased from an arbitrary prescribed initial value (for instance 10 kW·m^{-3}) to its continuously permissible value (corresponding to the temperature $T_{cp} = 90$°C). The volume powers of heat sources Q_v obtained in this manner are given in Table 8. Then, these volume powers of heat sources and (2) are used to calculate the cable ampacities. The ampacities I_{cp} of the considered 110 kV cable line are also given in Table 8.

Concerning the quantification of the effects of the pavement surface radiation properties and the cable bedding on the ampacity of the considered 110 kV cable line, the following can be noticed: (i) In comparison with the uncoated asphalt-pavement, the other materials can increase the ampacity of the considered 110 kV cable line by 88.393 A. (ii) The cable bedding having dimensions 1.2 m × 1.6 m can additionally increase the cable ampacity by 88.056 A. This means that the cable ampacity can be increased by 176.449 A if the asphalt-pavement is coated with magnesium oxide white paint and if the cable trench is completely filled with the bedding material.

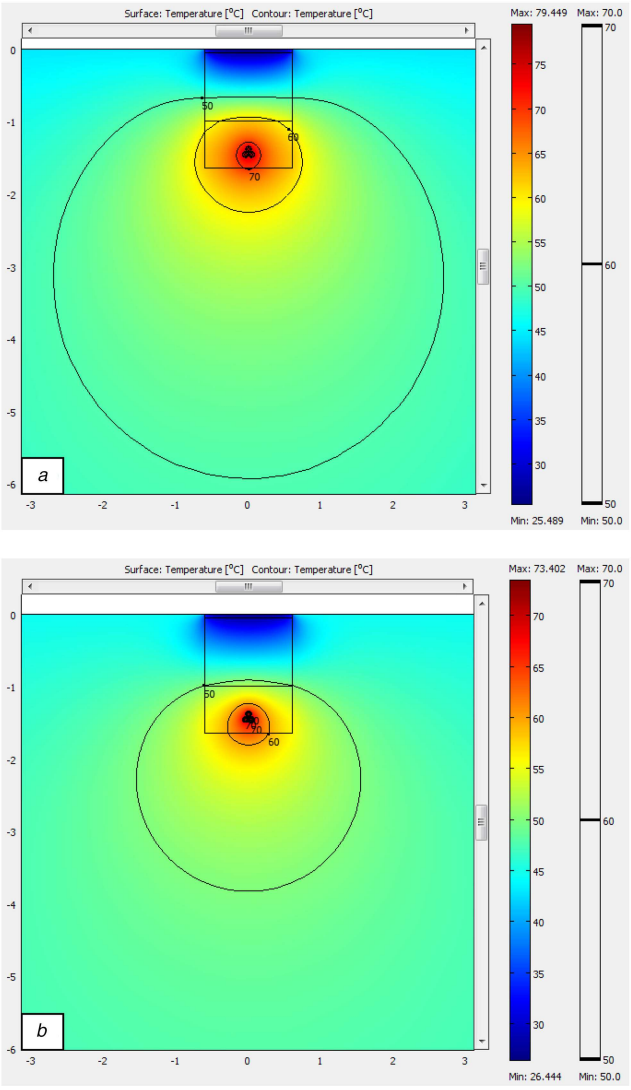

Fig. 8 *Isotherms of 50, 60 and 70°C surrounding the dried, dried-out and extremely dried-out zones around the 110 kV cables which are laid in accordance with*
(a) Fig. 5*a*, ***(b)***Fig. 5*b*, where all dimensions are in meters

5 Conclusions

The most important conclusions that can be drawn from the presented results are:

- After performing experimental tests and numerical simulations with white, grey and black pavement surfaces having approximately the same thermal emissivities and the following solar absorptivities: 0.26, 0.56 and 0.97; it is found that the load current of the single AXLJ 1 × 1000/190 mm^2 110 kV cable can be increased up to 25% for given ambient conditions if the effect of solar radiation is excluded.
- If the pavement over the cables is coated with magnesium oxide white paint or made of a material whose surface absorbs less heat from the Sun than it emits to the ambient, then the ampacity of the considered AXLJ 1 × 1000/190 mm^2 110 kV cables can be increased by 6.7–26.7%.
- Experimental and numerical results are in good agreement; therefore, the proposed method for controlling the thermal environment of underground cable lines and corresponding thermal FEM models can be used by electric power companies.
- It is found that the pavement made of concrete blocks covered by some river sand acting as dust has the same radiation properties as a clean and rough surface of the concrete block pavement. This is also verified by means of the FLIR i3 thermal imaging camera.
- All solid materials and white paints that have absorptivity-to-emissivity ratios of below 0.6 can be used for controlling the thermal environment of underground cable lines in distribution networks.
- Regardless of computational domain, the temperatures of the pavement, bedding and cables' conductors decrease with decreasing the ratio of absorptivity to emissivity.
- The effect of the pavement surface radiation properties on heat transfer between the cables and the air contacting the pavement surface is most significant when the cable trench is completely filled with the bedding material.
- The effect of the cable bedding on an underground cable line can best be illustrated using the 50, 60 and 70°C isotherms and the sizes of the dried, dried-out and extremely-dried-out zones enclosed by these isotherms.

Table 8 Volume powers of heat sources located in cables' conductors and cables' ampacities calculated for different pavement surface radiation properties and thermal environments

Pavement material	α/ε, —	Computational domain			
		Fig. 5*a*		Fig. 5*b*	
		Q_v W·m^{-3}	I_{cp} A	Q_v W·m^{-3}	I_{cp} A
asphalt + paint	0.100	13,890	627.058	18,065	715.114
brick, light	0.294	12,930	605.000	16,265	678.553
limestone, light	0.367	12,680	599.123	15,815	669.100
concrete block	0.596	11,660	574.521	13,915	627.622
asphalt	0.935	10,250	538.665	11,260	564.580

- Application of the proposed method would lead to the elimination of all possible hot spots caused by unfavourable conditions in the soil along a distribution cable line route.
- The proposed method for controlling the thermal environment of underground cable lines is new, it does not have to be too expensive, it can be easily implemented within current practice and it would result in significant economic benefits.

In addition to this last conclusion, the proposed method may not be as cheap as possible due to the following: (i) It will require periodic maintenance and cleaning to preserve the pavement surface radiation properties, especially in suburban and rural areas. (ii) Compared with the dimensionally optimised cable bedding, it requires up to 2.5 times higher volume of the bedding material. (iii) When the cable trench is completely filled with the bedding material, up to 2.5 times higher volume of the native soil must be transported to other places. Such method will definitely increase the costs of installation and maintenance. However, for the same price of the 110 kV cables and all the associated equipment, a significantly higher ampacity will be provided.

6 Acknowledgment

This paper was based on research conducted within the project TR33046.

7 References

[1] Al-Saud, M.S., El-Kady, M.A., Findlay, R.D.: 'A new approach to underground cable performance assessment', *Electr. Power Syst. Res.*, 2008, **78**, (5), pp. 907–918

[2] Nahman, J., Tanaskovic, M.: 'Calculation of the ampacity of high voltage cables by accounting for radiation and solar heating effects using FEM', *Int. Trans. Electr. Energy Syst.*, 2013, **23**, (3), pp. 301–314

[3] Klimenta, D., Nikolajević, S., Sredojević, M.: 'Controlling the thermal environment in hot spots of buried power cables', *Eur. Trans. Electr. Power*, 2007, **17**, (5), pp. 427–449

[4] Dubitsky, S., Greshnyakov, G., Korovkin, N.: 'Multiphysics finite element analysis of underground power cable ampacity'. Proc. 2014 Int. Conf. Energy, Environment and Material Science (EEMAS '14), Saint Petersburg, Russia, 23–25 September 2014, pp. 84–89

[5] Rerak, M., Ocłoń, P.: 'The effect of soil and cable backfill thermal conductivity on the temperature distribution in underground cable system'. 2017, vol. 13, Article No. 02004, E3S Web Conf., 4th Scientific and Technical Conference on Modern Technologies and Energy Systems, WTiUE, Cracow, Poland, October 2016, pp. 1–6, doi: 10.1051/e3sconf/20171302004

[6] Klimenta, D., Perovic, B., Jevtic, M.*, et al.*: 'A thermal FEM-based procedure for the design of energy-efficient underground cable lines', *Humanities Sci. Univ. J. Technics*, 2014, **10**, pp. 162–188

[7] International Standard IEC 60287–1-1:2006+AMD1:2014 CSV: '*Electric cables – calculation of the current rating – part 1-1: current rating (100% load factor) and calculation of losses – General*' (International Electrotechnical Commission, Switzerland, 2014, 2.1 edn.)

[8] COMSOL: 'Heat transfer module user's guide', Version 4.3, May 2012

[9] Çengel, Y.A.: '*Introduction to thermodynamics and heat transfer*' (The McGraw-Hill Companies Inc., USA, 2008, 2nd edn.)

[10] Andersland, O.B., Ladanyi, B.: '*Frozen ground engineering*' (John Wiley & Sons, Hoboken, NJ, USA, 2003, 2nd edn.)

[11] Seemann, S.W., Borbas, E.E., Knuteson, R.O.*, et al.*: 'Development of a global infrared land surface emissivity database for application to clear sky sounding retrievals from multispectral satellite radiance measurements', *J. Appl. Meteorol. Climatol.*, 2008, **47**, pp. 108–123

[12] Tan, S.-A., Fwa, T.-F.: 'Influence of pavement materials on the thermal environment of outdoor spaces', *Build. Environ.*, 1992, **27**, (3), pp. 289–295

[13] Smith, J.O.: 'Determination of the convective heat transfer coefficients from the surfaces of buildings within urban street canyons'. PhD thesis, University of Bath, 2010

[14] Herb, W.R., Janke, B., Mohseni, O.*, et al.*: 'All-weather ground surface temperature simulation'. Project Report No. 478, St. Anthony Falls Laboratory, University of Minnesota, September 2006

[15] Gouda, O.E., Amer, G.M., El Dein, A.Z.: 'Effect of dry zone formation around underground power cables on their ratings'. 20th Int. Conf. Electricity Distribution, Session 1, Paper 0120, Prague, Czech Republic, June 2009

[16] Gouda, O.E., El Dein, A.Z., Amer, G.M.: 'Effect of the formation of the dry zone around underground power cables on their ratings', *IEEE Trans. Power Deliv.*, 2011, **26**, (2), pp. 972–978